Translational Oncology 13 (2020) 100832

Contents lists available at ScienceDirect

Translational Oncology

journal homepage: www.elsevier.com/locate/tranon

Plocabulin, a novel tubulin inhibitor, has potent antitumor activity in patient-derived xenograft models of gastrointestinal stromal tumors

Yannick Wang [a,*], Agnieszka Wozniak [a], Jasmien Wellens [a], Yemarshet K. Gebreyohannes [a], Maria Jose Guillén [b], Pablo M. Avilés [b], Maria Debiec-Rychter [c], Raf Sciot [d], Patrick Schöffski [a,e]

[a] Laboratory of Experimental Oncology, Department of Oncology, KU Leuven, Leuven, Belgium
[b] PharmaMar S.A., Madrid, Spain
[c] Department of Human Genetics, KU Leuven and University Hospitals Leuven, Leuven, Belgium
[d] Department of Pathology, KU Leuven and University Hospitals Leuven, Leuven, Belgium
[e] Department of General Medical Oncology, University Hospitals Leuven, Leuven, Belgium

ARTICLE INFO

Article history:
Received 14 April 2020
Accepted 16 June 2020
Available online xxxx

Keywords:
Gastrointestinal stromal tumor
Patient-derived xenograft
Plocabulin
PM060184
Tubulin inhibitor

ABSTRACT

The majority of patients with gastrointestinal stromal tumors (GIST) eventually become resistant with time due to secondary mutations in the driver receptor tyrosine kinase. Novel treatments that do not target these receptors may therefore be preferable. For the first time, we evaluated a tubulin inhibitor, plocabulin, in patient-derived xenograft (PDX) models of GIST, a disease generally considered to be resistant to cytotoxic agents. Three PDX models of GIST with different *KIT* genotype were generated by implanting tumor fragments from patients directly into nude mice. We then used these well characterized models with distinct sensitivity to imatinib to evaluate the efficacy of the novel tubulin inhibitor. The efficacy of the drug was assessed by volumetric analysis of the tumors, histopathology, immunohistochemistry and Western blotting. Plocabulin treatment led to extensive necrosis in all three models and significant tumor shrinkage in two models. This histological response can be explained by the drug's vascular-disruptive properties, which resulted in a shutdown of tumor vasculature, reflected by a decreased total vascular area in the tumor tissue. Our results demonstrated the *in vivo* efficacy of the novel tubulin inhibitor plocabulin in PDX models of GIST and challenge the established view that GIST are resistant to cytotoxic agents in general and to tubulin inhibitors in particular. Our findings provide a convincing rationale for early clinical exploration of plocabulin in GIST and warrant further exploration of this class of drugs in the management of this common sarcoma subtype.

Introduction

Gastrointestinal stromal tumors (GIST) are the most common mesenchymal tumors of the gastrointestinal tract [1]. Patients in the pre-imatinib era faced a dire prognosis: early reports suggested that more than half of all GIST would recur after surgery and that most patients would eventually die of their disease [2,3]. However, specific immunohistochemical KIT positivity [4] and gain-of-function mutations in the *KIT* oncogene, encoding for constitutively activated receptor tyrosine kinases as key drivers in GIST, were reported in 1998 [5]. This insight revolutionized the treatment for GIST. Imatinib, a tyrosine kinase inhibitor (TKI) with multi-target specificity against KIT, BCR-ABL and platelet-derived growth factor receptor alpha (PDGFRA), was tested in patients with advanced GIST and proved to be highly effective [6,7]. Subsequently, imatinib, and later newer generations of TKI, have become standard of care for patients with locally advanced, unresectable or metastatic GIST, and for patients with a high risk of recurrence after primary surgery. This practice is further supported by more recent observations that 80–95% of GIST are either driven by oncogenic mutations in *KIT* (70–80% of cases) or *PDGFRA* (10–14% of cases), a homologous receptor tyrosine kinase [8,9]. Due to the introduction of TKI in the management of GIST, the median overall survival for patients with advanced and metastatic GIST has greatly increased in the past three decades from under 2 years to almost 7 years more recently. [2,10]

Despite these major advancements, practically all patients with inoperable and metastatic GIST progress due to the development of resistance to imatinib, mainly because of secondary mutations in the *KIT* gene [11,12]. Further treatment options are available for patients who are imatinib resistant (either primary or secondary due to acquired resistance) or intolerant — sunitinib and regorafenib are TKI used in second- and third-line treatment of GIST, respectively. However, with each line of treatment there is a diminishing return of quality, magnitude and duration of disease control [13–15]. Patients who have failed these three lines of treatment are currently left with no approved therapeutic options. A few novel tyrosine

* Corresponding author at: Laboratory of Experimental Oncology, Department of Oncology, KU Leuven, Herestraat 49, box 815, 3000 Leuven, Belgium.
E-mail address: yannick.wang@kuleuven.be. (Y. Wang).

http://dx.doi.org/10.1016/j.tranon.2020.100832

kinase inhibitors are currently still being investigated in clinical trials [16,17]. Rechallenge with imatinib or sunitinib only provides a short duration of clinical benefit in some patients. Previous trials reported median progression-free survival and median time of progression of 1.8 and 5.4 months in retreated patients, respectively [18,19]. Systemic treatment with chemotherapy based on non-TKI, cytotoxic agents have proven ineffective in GIST in the pre-imatinib era when not any effective, targeted therapy was known for unresectable or metastatic GIST. Extremely low response rates of around 5% were observed with this class of drugs in GIST [20,21]. This was further demonstrated in a study by Verweij and colleagues, showing a dismal overall survival of patients treated with doxorubicin-based chemotherapy when compared to those treated with imatinib [22]. Local treatment, such as ablations or palliative radiotherapy is not curative and only indicated in selected patients [23].

In light of this, there is an urgent need for testing and developing novel treatment options for these patients, whose general condition often still permits further systemic therapy, even after multiple lines of treatment with TKI. Novel treatments that do not target the driver oncogenic kinases may be preferable, taken into account that resistance to TKI is mainly caused by secondary mutations of these kinases and that consecutive lines of treatment with TKI result in diminishing disease control. In contrast to previous data that showed limited efficacy of cytotoxic agents in the management of GIST, more recent data however, suggest that some cytotoxic agents may actually have activity against this disease [24].

Plocabulin (PM060184, PharmaMar) is a novel tubulin binding agent, originally isolated from the marine sponge *Lithoplocamia lithiostoides*. It targets the recently described maytansine site on β-tubulin and showed potent antitumor activity both *in vitro* and *in vivo*, through inhibition of microtubule polymerization and dynamics [25–27]. In dividing cells, it induces multipolar spindles and lagging chromosomes in metaphase, as an intact spindle apparatus is critical for the proper alignment and separation of chromosomes during mitosis. In interphase cells, where unimpaired microtubules are critical for cell shape, trafficking, signaling, transportation and migration, it leads to microtubule disorganization and fragmentation. This initiates prometaphase cell arrest and induces caspase-dependent apoptosis [28]. Recent studies also demonstrated antiangiogenic properties of plocabulin, which caused a strong reduction in vascular volume both *in vitro* and *in vivo* [29]. Moreover, a recent phase I study demonstrated promising antitumor effects in patients with advanced solid tumors [28]. Currently, plocabulin is being further assessed in additional, early clinical trials [30–33].

In the currently presented preclinical study, we investigated the *in vivo* efficacy of plocabulin in GIST using three patient-derived xenografts (PDX) carrying different *KIT* mutations, conferring distinct sensitivities to imatinib.

Material and methods

Establishment of xenografts

Six-week-old, female, athymic Rj:NMRI-*Foxn1*$^{nu/nu}$ mice were supplied by Janvier Labs. Xenografts were established by bilateral implantation of a human tumor fragment subcutaneously as described previously [34]. In brief, fresh tumor samples from donor patients were cut into fragments of ±10 mm^3. A 0.5–1 cm skin incision was made on each flank of an immunodeficient mice, anesthetized using a 3% isoflurane mixture in oxygen, and one tumor piece was inserted subcutaneously on each side of the animal. Wounds were then closed with 6–0 silk sutures (Mersilk, Ethicon). Mice were sacrificed once tumor volumes reached approximately 700–1000 mm^3. After removal of the tumors, fragments were retransplanted to a next generation of mice (n = 2–3). This process of 'passaging' was repeated to maintain the model. With every passage, morphology was checked and immunohistochemistry was performed to characterize the models. A model was considered as 'established' when stable histological and molecular features were confirmed for at least two passages. The Medical Ethics Committee of the University Hospitals Leuven approved the collection of human tumor tissue and its usage for xenograft work (approval number: S53483). All donor patients gave written informed consent to the usage of their tumor tissue. The Animal Ethics Committee of KU Leuven approved the creation of the PDX models and the *in vivo* experiments (approval number: P175-2015), which were performed according to its guidelines and Belgian regulations.

Drug preparation

Imatinib mesylate was purchased from Sequoia Research and its working solution was prepared with sterile water. Plocabulin and vehicle were obtained from PharmaMar as lyophilized vials and prepared according to the manufacturer's instructions to reach the target concentrations. Vehicle was used as the nonactive treatment in control mice. All solutions were brought to room temperature before administration.

Treatment design

Three GIST PDX models with different sensitivity to imatinib, UZLX-GIST3$^{KIT\ 11}$, UZLX-GIST9F$^{KIT\ 11+17}$ and UZLX-GIST2BF$^{KIT\ 9}$, were used to assess the *in vivo* efficacy of plocabulin. UZLX-GIST3$^{KIT\ 11}$, harboring mutation in *KIT* exon 11, is sensitive to imatinib. UZLX-GIST9F$^{KIT\ 11+17}$, harboring mutations in *KIT* exon 11 and 17, is resistant to imatinib. UZLX-GIST2BF$^{KIT\ 9}$, harboring mutation in *KIT* exon 9 is resistant to imatinib in a dose-dependent manner. For model expansion, 62 mice were implanted subcutaneously with human tumor fragments under general anesthesia with a xylazine/ketamine mixture injected intraperitoneally. Each mouse was engrafted with tumors from a single model. Ultimately, 80 tumors were generated in 49 mice. Randomization of mice and the first administration of drug were initiated 9 weeks after engraftment for UZLX-GIST3$^{KIT\ 11}$ and UZLX-GIST9F$^{KIT\ 11+17}$, and 19 weeks after engraftment for UZLX-GIST2BF$^{KIT\ 9}$ due the slower growth characteristics of this model. Mice were randomized into three treatment groups for UZLX-GIST3$^{KIT\ 11}$ and UZLX-GIST9F$^{KIT\ 11+17}$: 1) vehicle 5 ml/kg once every week, 2) imatinib 50 mg/kg twice daily, or 3) plocabulin 16 mg/kg once every week. Mice bearing UZLX-GIST2BF$^{KIT\ 9}$ were randomized into two groups, comprising the vehicle group and the plocabulin group. Vehicle and plocabulin were delivered by i.v. bolus injection into the lateral tail veins. Imatinib was administered orally using a flexible gavage needle. During treatment, which lasted 22 days, tumors were measured three times per week using digital calipers. Body weight was measured daily and the animals' wellbeing was checked daily. On the final day of the experiment, day 22 of drug exposure, all mice were sacrificed by cervical dislocation after an intraperitoneal overdose of pentobarbital sodium (Vetoquinol). Tumors were collected, partly snap frozen in liquid nitrogen, and partly fixed in 10% neutral buffered formalin for further analysis.

Tumor volume measurement

Tumor volume was calculated as width x length x height, with length defined as the greatest dimension and the other two axes perpendicular to the previous one. Tumors with starting volume < 100 mm^3 on the first day of drug exposure were excluded from volumetric analysis. Tumors from mice receiving active treatment, imatinib and plocabulin, were excluded from tumor volume analysis if they were collected before the final day of the experiment.

Immunohistochemistry

Fixed tumors were embedded in paraffin and 4 μm sections were cut for hematoxylin and eosin (H&E) and immunohistochemical staining. Preparations were dried for 1 h at 58 °C, then overnight at 37 °C. Tissue sections were deparaffinized and rehydrated in UltraClear™ (Klinipath) and ethanol series respectively. Endogenous peroxidase activity was quenched by a 20-min treatment with 0.09% hydrogen peroxidase dissolved in methanol (except for CD31 staining, for which a 15-min treatment with 0.9% hydrogen

peroxidase dissolved in distilled water was used). Epitopes were unmasked with heat-induced epitope retrieval. Citrate buffer (pH = 6.0) was used as retrieval buffer for phospho-histone H3 (pHH3) and Ki-67. Tris-EDTA buffer was used for CD31 and Discovered On GIST1 (DOG-1). Reveal Decloaker (Biocare Medical) was used for cleaved poly-ADP-ribose-polymerase (cleaved PARP). No antigen retrieval was carried out for KIT. The following primary antibodies were used: CD31 (clone SZ31, DIA-310, Dianova), KIT (A450229-2, Agilent), cleaved PARP (clone 5E1, ab32064, Abcam), DOG-1 (clone K9, NCL-L-DOG-1, Leica Biosystems), HLA-A (clone EP1395Y, ab52922, Abcam), Ki-67 (clone SP6, MA5-14520, Thermo Fisher Scientific) and pHH3 (9701, Cell Signaling Technologies). Antigen-antibody complexes were visualized using diaminobenzidine (Dako), incubated for 10 min, and slides were counterstained with Gill's hematoxylin (VWR).

Histological assessment

Histologic response (HR) was graded as previously described for TKI response, by assessing the percentage of necrosis, myxoid degeneration and/or fibrosis on H&E staining as follows: grade 1 (<10%), grade 2 (10–50%), grade 3 (50–90%) or grade 4 (>90%) [35]. Mitotic and apoptotic activity were evaluated by counting the number of mitotic figures and apoptotic cells in 10 high-power fields (HPF, 400-fold magnification, field of view diameter: 450 μm) on H&E. Ki-67 index was calculated as the average percentage of Ki-67 positive cells in five images taken at 400× magnification as described previously [36]. Immunohistochemistry for pHH3 and cleaved PARP were used as marker for proliferation and apoptosis, respectively, and was assessed by calculating the average number of positive cells in 10 HPF. To analyze the treatments' effects on the tumor vasculature, CD31 stains were assessed. The mean vascular density and total vascular area were defined as the average number of vessels and the average area those vessels covered on five digital micrographs captured at 200× magnification (0.24 mm^2 area), respectively. Individual microvessels were identified as described previously [37]. Histological analysis was performed using CH30 Binocular Microscope (Olympus) and images were analyzed using cellSense Dimension software (Olympus, version 1.16). Tumors from mice in the imatinib and plocabulin group that were sacrificed before the end of experiment were excluded from all histological assessment.

Western blotting

For each PDX model, four tumors were randomly selected and tumor lysates were prepared from snap frozen tumor fragments as described previously [38]. The lysates were then loaded on NuPAGE™ 4%–12% Bis-Tris Gels (ThermoFisher Scientific) and electrophoresed using NuPage™ MOPS SDS Running Buffer (ThermoFisher Scientific) at 150 V for 2 h. Four different tumor lysates were used per treatment group. Samples were then blotted on polyvinylidene fluoride membranes (Bio-Rad) in a semi-dry transfer at 25 V for 30 min, using a transfer buffer with 20% methanol, 25 mM tromethamine and 190 mM glycine. The following primary antibodies were used: KIT (A450229-2, Agilent), phospho-KIT Tyr719, phospho-KIT Tyr703, AKT, phospho-AKT Ser743, p44/42 mitogen-activated protein kinase (MAPK), phospho-p44/42 MAPK Thr202/Tyr204, eukaryotic translation initiation factor 4E binding protein 1 (4E-BP1), phospho-4E-BP1 Ser65, ribosomal protein S6, phospho-S6 Ser240/244 and α-tubulin (catalogue numbers: 3391, 3073, 7292, 7291, 9102, 4370, 9644, 9456, 2217, 5364 and 2144, respectively; all from Cell Signaling Technology). Horseradish peroxidase conjugated secondary polyclonal goat antirabbit immunoglobulins (P044801, Agilent) were added and specific bands were visualized using Western Lightning™ ECL Pro kit (Perkin Elmer). Chemiluminescence was captured using the FUJI-LAS mini 3000 system (Fujifilm).

Statistical analysis

GraphPad Prism 8 (GraphPad Software) was used for analysis with $p < 0.05$ considered as statistically significant. Kruskal-Wallis' test with Dunn's multiple comparisons test as *post hoc* test was used for comparison of non-parametric variables of the different treatment groups (relative tumor volumes at end of experiment and histological analysis). The Mann-Whitney *U* test was used for data comprising only two groups. Absolute tumor volumes within groups at start and end of experiment were compared using the Wilcoxon matched-pairs signed rank test to assess tumor volume evolution. Two tumors engrafted on the same mouse were regarded as independent entities, as was demonstrated previously by our group and were thus analyzed separately [39].

Results

UZLX-GIST3$^{KIT\ 11}$, UZLX-GIST9F$^{KIT\ 11+17}$ and UZLX-GIST2BF$^{KIT\ 9}$ are histologically and molecularly stable models

All three models were established using tumor tissue from patients with GIST and showed stable histological characteristics. Model features and patient characteristics were described previously [34,40]. A comparison of the original patient tumor and passages used in the *in vivo* experiment can be seen in Fig. 1. Consistent with previous reports, all three models showed spindle cell morphology and KIT and DOG-1 immunoreactivity, further confirming the GIST nature of the xenografts [38,40]. Mutational analysis confirmed that all models still harbor the same *KIT* mutation as the respective original patient samples from which the models were established (data not shown). UZLX-GIST3$^{KIT\ 11}$ harbored *KIT* mutation in exon 11 (p.W557_V559delinsF), UZLX-GIST9F$^{KIT\ 11+17}$ harbored mutations in exons 11 and 17 (p.P577del;W557LfsX5;Y823D) and UZLX-GIST2BF$^{KIT\ 9}$ harbored mutation in exon 9 (p.A502_Y503dup).

Plocabulin was well tolerated without severe toxicity observed

Overall, treatment with plocabulin was well tolerated without major body weight loss. Plocabulin-treated mice of UZLX-GIST3$^{KIT\ 11}$ reached 103% of starting body weight at the end of the experiment, while those of UZLX-GIST9F$^{KIT\ 11+17}$ reached 97% and those of UZLX-GIST2BF$^{KIT\ 9}$ reached 98%. One plocabulin-treated mouse of UZLX-GIST3$^{KIT\ 11}$ was sacrificed on day 10 due to a 20% loss body weight loss. However, it already had a low bodyweight of 30 g on the first day of drug exposure (the average body weight across all groups was 33 g). In the UZLX-GIST9F$^{KIT\ 11+17}$ model, two plocabulin-treated mice were sacrificed. One mouse that had a very low body weight of 26 g at the start of drug exposure was sacrificed on day three because of a 19% body weight loss. The other mouse, with a normal body weight at the start of drug exposure, was sacrificed on day 21 for a body weight loss of 23%. An overview of the body weight evolution can be found in Supplementary Fig. S1.

Plocabulin led to a statistically significant tumor volume decrease in UZLX-GIST3$^{KIT\ 11}$ and UZLX-GIST9F$^{KIT\ 11+17}$

Vehicle-treated tumors reached 124%, 191% and 169% of baseline volume after 22 days of drug exposure for UZLX-GIST3$^{KIT\ 11}$, -GIST9F$^{KIT\ 11+17}$ and -GIST2BF$^{KIT\ 9}$, respectively. However, none of these changes were statistically significant.

Plocabulin treatment resulted in statistically significant tumor regression in UZLX-GIST3$^{KIT\ 11}$ and UZLX-GIST9F$^{KIT\ 11+17}$. Tumors of UZLX-GIST3$^{KIT\ 11}$ treated with plocabulin shrank to 64% of baseline volume ($p = 0.02$, Wilcoxon matched-pairs signed rank test, WMP), while those of UZLX-GIST9F$^{KIT\ 11+17}$ shrank to 44% ($p = 0.03$, WMP). Plocabulin-treated tumors of UZLX-GIST2BF$^{KIT\ 9}$ also decreased in size, to 81% of baseline volume. This change was not statistically significant. However, the end relative tumor volumes differed significantly between the vehicle group and plocabulin group ($p = 0.016$, Mann Whitney *U* test).

Expectedly, imatinib treatment resulted in tumor volume reduction in UZLX-GIST3$^{KIT\ 11}$, the imatinib-sensitive model with *KIT* exon 11 mutation, while having no effect on UZLX-GIST9F$^{KIT\ 11+17}$, the model with double *KIT* exon 11 and 17 mutations. After 22 days of drug exposure, tumor

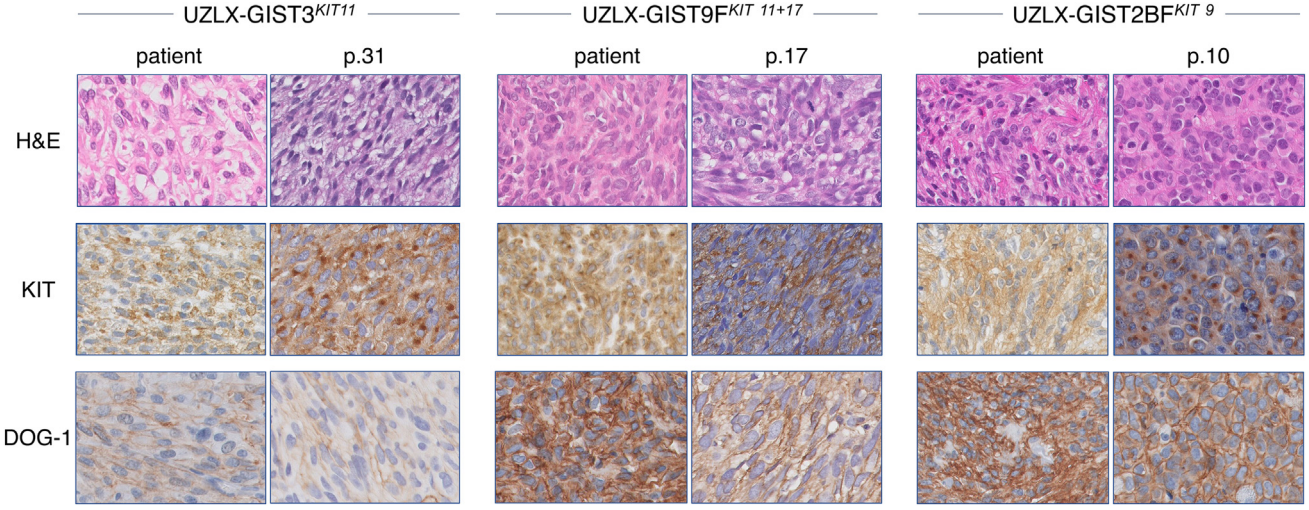

Fig. 1. UZLX-GIST3$^{KIT\ 11}$, UZLX-GIST9F$^{KIT\ 11+17}$ and UZLX-GIST2BF$^{KIT\ 9}$ are stable models, retaining their original morphology and immunohistochemical profile. All three models stain positively for KIT and DOG-1, confirming their GIST nature. Images captures at 400× magnification. DOG-1: Discovered on GIST 1; H&E: hematoxylin-eosin; p.: passage.

volume decreased to 18% of baseline in the sensitive model ($p = 0.03$, WMP). Imatinib treated tumors of UZLX-GIST9F$^{KIT\ 11+17}$ reached 169% of baseline volume. Detailed results are presented in Fig. 2 and Table 1.

Placobulin reduced the total vascular area in UZLX-GIST3$^{KIT\ 11}$ and UZLX-GIST2BF$^{KIT\ 9}$, and induced extensive necrosis in all three models

Placobulin treated tumors were highly necrotic. As Fig. 3 and Supplementary Fig. S2 illustrate, large parts of the tumors were replaced by white-yellow debris, which was already visible to the naked eye. Indeed, microscopic analysis showed that placobulin induced an excellent response in 70%, 50% and 43% of tumors of UZLX-GIST3$^{KIT\ 11}$, -GIST9F$^{KIT\ 11+17}$ and -GIST2BF$^{KIT\ 9}$, respectively. This response was characterized by extensive, central necrosis, leaving behind a small rim of viable tumor at the periphery of the tumors. Conversely, imatinib's effect on UZLX-GIST3$^{KIT\ 11}$ was characterized by myxoid degeneration, matching the typical response that is seen in GIST treated with imatinib clinically and our earlier experience with the TKI in our GIST xenograft models. All imatinib treated tumors of UZLX-GIST3$^{KIT\ 11}$ showed complete myxoid degeneration, a process in which viable tumor tissue is replaced by an amorphous, myxoid matrix, with a few scattered cells throughout it. Consequently, none of those tumors could be evaluated histologically as originally planned. Expectedly, UZLX-GIST9F$^{KIT\ 11+17}$ did not show enhanced histological response to imatinib when compared to vehicle.

To explain the observed tumor volume regression and pronounced necrosis, we performed further histologic analyses to determine the mechanism of the response. However, the placobulin groups could only be partially evaluated due to the very extensive necrosis. Fig. 4 shows a detailed overview of the results of the histological analysis.

Analysis of the effect of placobulin on proliferation, based on H&E, pHH3 and Ki-67 immunostaining, was not conclusive. Immunostaining of pHH3 showed that placobulin yielded a 1.48-fold increase in pHH3-positive cells in UZLX-GIST3$^{KIT\ 11}$ ($p = 0.048$, Mann-Whitney U test). However, assessment of the number of mitotic figures and Ki-67 index did not show a significant difference between the groups. The increase in the number of pHH3 positive cells could not be observed in UZLX-GIST2BF$^{KIT\ 9}$. As only one tumor in the placobulin group of UZLX-GIST9F$^{KIT\ 11+17}$ could be assessed for pHH3 by immunohistochemistry, subsequent statistical analysis of that model was not carried out.

Assessment of the apoptotic activity showed a similar pattern. Placobulin treatment resulted in a 1.51-fold increase in the number of apoptotic cells based on immunostaining of cleaved PARP. However, this increase in apoptotic activity was only observed in UZLX-GIST3$^{KIT\ 11}$ and could not be confirmed by H&E staining by assessing the number of apoptotic bodies.

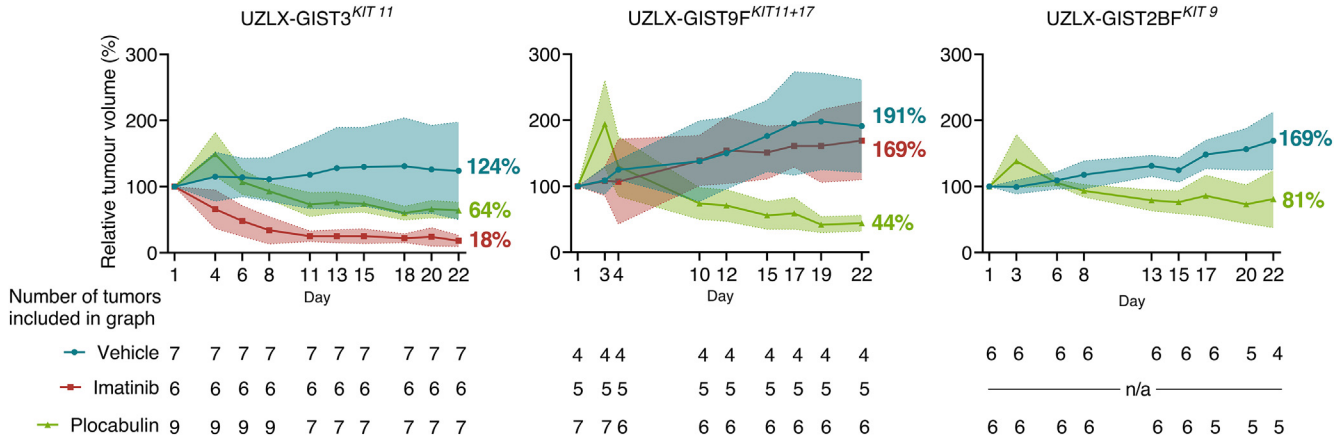

Fig. 2. Evolution of the tumor volumes over 22 days of drug exposure. Data displayed as average relative tumor volume compared to baseline with 95% confidence interval (shaded). The number of tumors included in the graph on any day is indicated.

Table 1
Plocabulin treatment resulted in statistically significant tumor regression in UZLX-GIST3$^{KIT\ 11}$ and UZLX-GIST9F$^{KIT\ 11+17}$. Detailed overview of the average absolute tumor volumes and average relative tumor volumes per group. Significant *p*-values are underlined.

Xenograft model	Group	Average absolute tumor volume		p-Value compared to day 1 (WMP)	Average relative tumor volume		p-Value compared to vehicle (DMC)	p-Value compared to imatinib (DMC)
		Day 1 (range), mm^3	Day 22 (range), mm^3		Day 22 (95% CI), %	p-Value of Kruskal-Wallis test		
UZLX-GIST3$^{KIT\ 11}$	Vehicle	201.6 (106.9–408.8)	275.1 (6.5–664.2)	0.219	124 (50–198)		n/a	0.024
	Imatinib	436.5 (158.2–814.7)	68.7 (30.6–103.5)	0.031	18 (10–26)	0.015	0.024	n/a
	Plocabulin	387.3 (152.8–649.4)	260.1 (104.9–514.3)	0.016	64 (52–76)		>0.999	0.100
UZLX-GIST9F$^{KIT\ 11+17}$	Vehicle	435.5 (235.9–570.0)	864.0 (368.52–1383.59)	0.125	191 (121–261)		n/a	>0.999
	Imatinib	867.7 (220.8–1915.5)	1714.2 (275.83–4515.26)	0.063	169 (110–228)	<0.001	>0.999	n/a
	Plocabulin	713.5 (210.3–1364.9)	289.0 (99.6–672.23)	0.031	44 (32–56)		0.013	0.033
UZLX-GIST2BF$^{KIT\ 9}$	Vehicle	1173.1 (366.0–2573.8)	1661.7 (695.2–2219.1)	0.125	169 (126–213)	n/a	n/a	n/a
	Plocabulin	1035.2 (234.4–3496.7)	713.5 (257.8–2304.5)	0.313	81 (38–124)		0.016*	n/a

CI: confidence interval; DMC: Dunn's multiple comparisons test; n/a: not available; WMP: Wilcoxon matched-pairs signed rank test. *Mann-Whitney U test instead of Dunn's multiple comparisons test.

Unable to explain the mechanism behind the histologic response induced by plocabulin, we then investigated any possible effect on the tumor vasculature. To visualize the tumor vasculature, we performed CD31 stains using a primary antibody that specifically targets the murine epitope without cross-reaction with the human counterpart. These stains showed a decrease in the total vascular area without an effect on the mean vascular density in both UZLX-GIST3$^{KIT\ 11}$ and UZLX-GIST2BF$^{KIT\ 9}$. Tumors of the vehicle group, compared to those of the plocabulin group, contained more clearly discernible microvessels with a larger diameter, often with a dilated lumen containing erythrocytes. Plocabulin-treated tumors, on the other hand, contained shorter and smaller microvessels with a collapsed lumen (Fig. 5). Again, only a single plocabulin-treated tumor of UZLX-GIST9F$^{KIT\ 11+17}$ could be evaluated due to extensive necrosis of the other specimens.

Plocabulin did not affect KIT signaling

Western blotting was performed to study the effects on KIT activation and signaling. As Supplementary Fig. S3 illustrates, plocabulin-treated tumors did not show altered KIT signaling, consistent with its mechanism of action – being a tubulin inhibitor and not a tyrosine kinase inhibitor. Vehicle-treated tumors of both models showed expression of KIT and downstream substrates, which were activated in all three models. Expectedly, analysis of imatinib-treated tumors of UZLX-GIST3$^{KIT\ 11}$ showed strongly

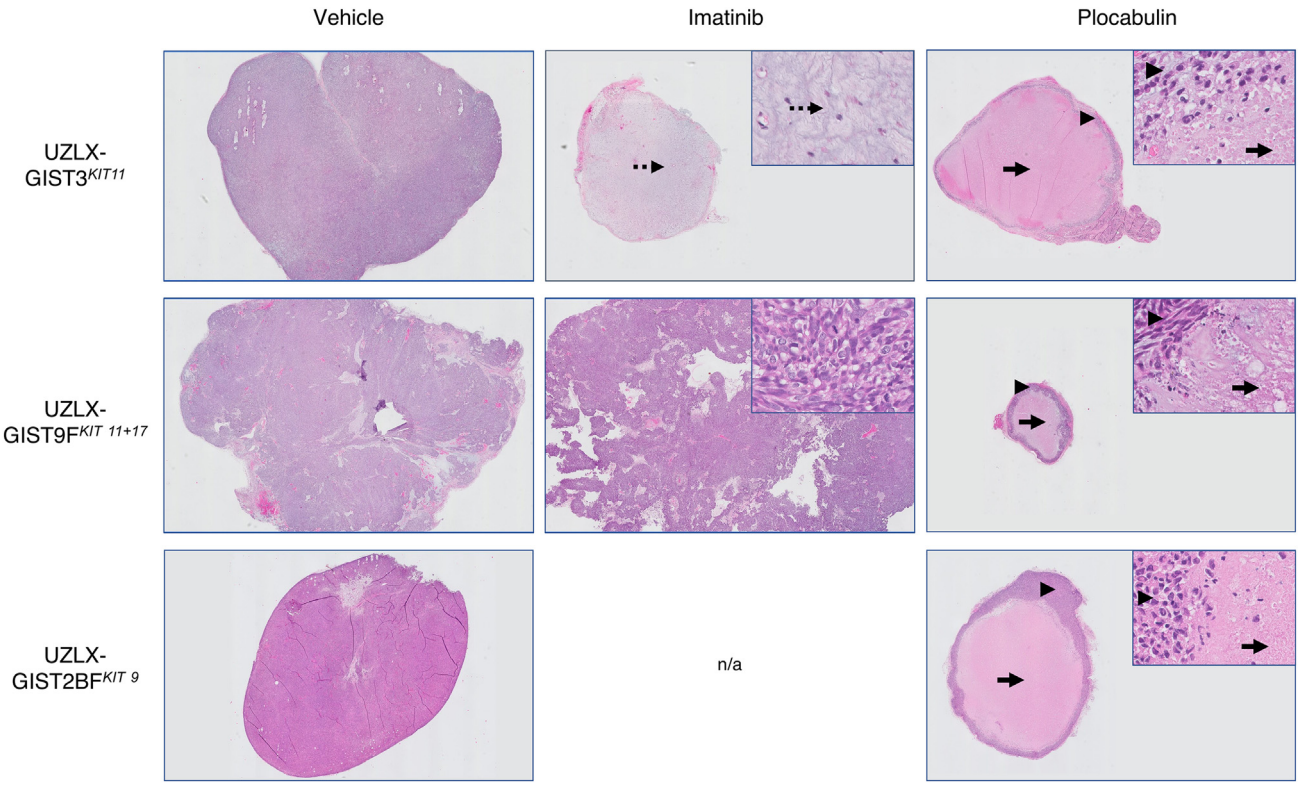

Fig. 3. Plocabulin induced extensive central tumor necrosis (full arrow), regardless of the models' sensitivity to imatinib. However, a small rim of viable tumor tissue remained at the periphery of the tumors (arrowheads). Imatinib caused a different type of response in the imatinib-sensitive model, UZLX-GIST3$^{KIT\ 11}$, which was characterized by myxoid degeneration (dashed arrow). Representative hematoxylin and eosin stains of tumors after 22 days of treatment. Images captured at 10× magnification (insets: 400×). n/a: not available.

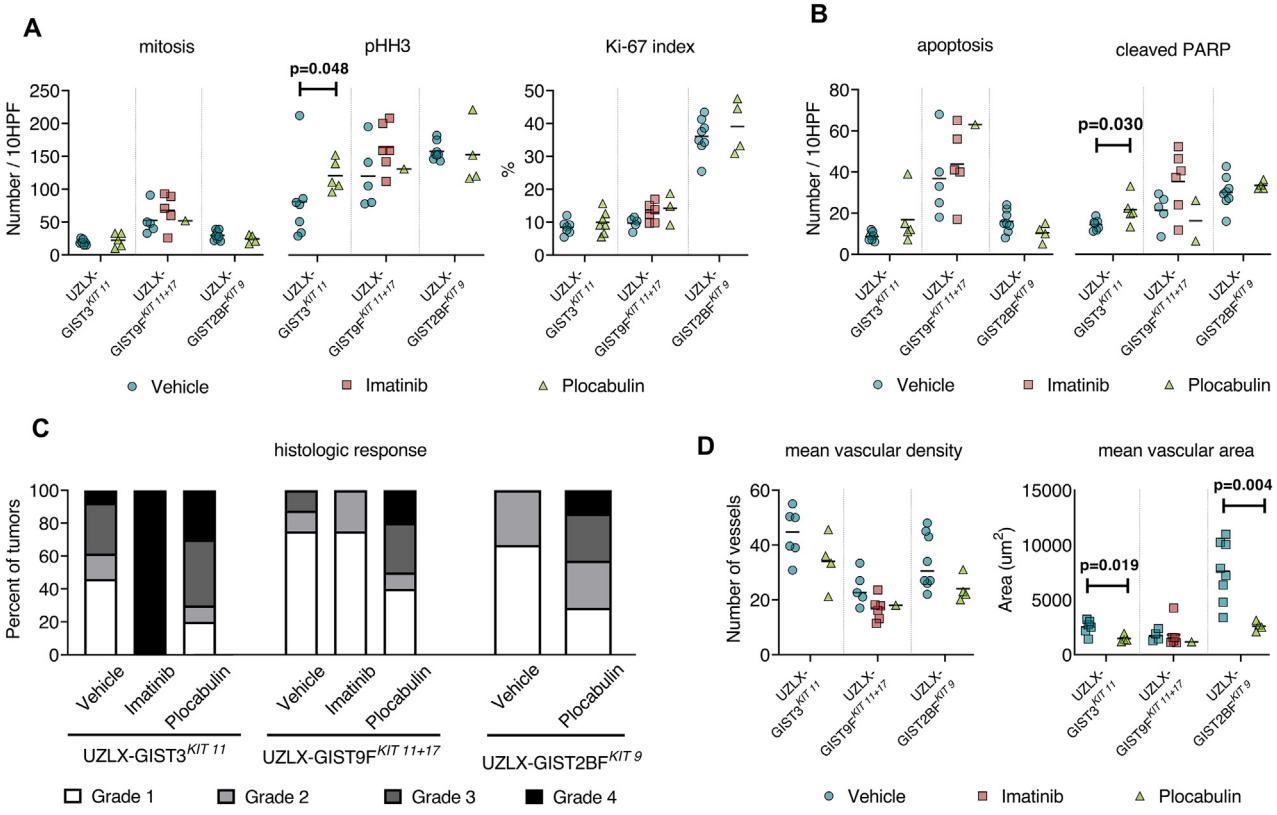

Fig. 4. Placobulin resulted in good histological response (grade 3 and grade 4) in more than 40% of tumors and showed vascular-disruptive activity leading to a decreased total vascular area. A, Proliferative activity. Placobulin-treated tumors of UZLX-GIST3$^{KIT\ 11}$ showed more phospho-histone H3 positive cells than vehicle-treated ones, albeit without a correlation with mitotic count or Ki-67 index. B, Apoptotic activity. Placobulin-treated tumors of UZLX-GIST3$^{KIT\ 11}$ showed more cleaved PARP positive cells than vehicle-treated ones, albeit without a correlation with the apoptotic count or the other evaluated models. C, Histologic response (HR) was graded by assessing the percentage of necrosis, myxoid degeneration and/or fibrosis follows: grade 1 (< 10%), grade 2 (10–50%), grade 3 (50–90%) or grade 4 (>90%) [35]. D, Angiogenesis. Tumor vasculature were visualized with a CD31-stain and the number area of those vessels were measured. Placobulin-treated tumors of both UZLX-GIST3$^{KIT\ 11}$ and UZLX-GIST2BF$^{KIT\ 9}$ showed a lower mean vascular area. Only one placobulin-treated tumor of UZLX-GIST9$^{KIT\ 11+17}$ could be evaluated due to extensive necrosis. Data presented as individual values per tumor with mean (horizontal line) per treatment group. Statistically significant differences are annotated. Displayed *p*-values were obtained in the Mann-Whitney *U* test. pHH3: phospho-histone H3; PARP: Poly (ADP-ribose) polymerase.

diminished protein expression, compatible with the greatly reduced cellularity of those tumors. Neither total KIT, nor the phosphorylated forms of it could be detected in these tumors. In the UZLX-GIST9F$^{KIT\ 11+17}$ model, imatinib treatment did not affect KIT activation or signaling, consistent with the model's *KIT* genotype.

Discussion

In the current *in vivo* study, we evaluated the efficacy of placobulin, a novel cytotoxic tubulin inhibitor, in three PDX models of GIST with different sensitivity to imatinib. All these models have been successfully used in previous *in vivo* experiments [38,41–43] and retain the morphological, immunohistochemical and molecular features of the original tumors, notwithstanding having been repeatedly passaged. Moreover, the imatinib-treated control groups of the current experiment behaved in a consistent way across the current and earlier experiments performed by our group [34,40].

Placobulin caused significant tumor regression in UZLX-GIST3$^{KIT\ 11}$ and UZLX-GIST9F$^{KIT\ 11+17}$, while in UZLX-GIST2BF$^{KIT\ 9}$ it did not. However, analysis showed a difference between the end relative tumor volumes of the vehicle and placobulin group in the latter model. This difference suggests that there actually was an effect of placobulin treatment on tumor volume in this model. Taking into account the relatively small number of tumors generated in that model, our experiment might not have had enough power to fully demonstrate that effect. Histological analysis showed an increase in pHH3 positive cells in UZLX-GIST3$^{KIT\ 11}$, thus suggesting that placobulin may have some pro-proliferative effects. However, neither did this finding correlate with the analysis of the H&E stains, which did not show an increase in mitotic figures, nor did it correlates with an increased Ki-67 index. It should be noted that phosphorylation of histone H3 is a marker of cell cycle progression from G2- to M-phase and that cells in cell cycle arrest show sustained phosphorylation of histone H3 [44,45]. Thus, the increased expression of phospho-histone H3 may be explained by a G2/M phase arrest, induced by placobulin.

The histologic type of response obtained with placobulin was characterized by extensive, central necrosis, with a small rim of viable tumor tissue remaining at the periphery of the tumor. This pattern is typically seen in solid tumors that have been treated with vascular disrupting agents [46]. The central part becomes necrotic as the tumor vasculature is shut down. Tumor cells at the periphery, however, may still obtain oxygen and nutrients from nearby vessels located in normal tissue surrounding the tumor [46]. Indeed, some of the placobulin-treated tumors of UZLX-GIST3$^{KIT\ 11}$ and UZLX-GIST2BF$^{KIT\ 9}$ could still be evaluated, despite the extensive necrosis. Those tumors showed a diminished total vascular area, albeit without significant change in total vascular density. Placobulin-treated tumors of the UZLX-GIST9F$^{KIT\ 11+17}$ model were necrotic to such an extent that made further analysis impossible in all but one tumor. Tumors in the vehicle group of UZLX-GIST3$^{KIT\ 11}$ contained larger vessel with a greater diameter, often with a clearly visible and dilated lumen containing erythrocytes. Placobulin-treated tumors, in contrast, harbored much smaller and shorter vascular structures, usually with collapsed, barely discernible lumina. These findings suggest that vascular-disruptive properties of placobulin also contribute to its antitumor effect. This hypothesis is supported by previous studies. Galmarini and colleagues explored the antiangiogenic and vasodisruptive effects of placobulin and demonstrated that placobulin

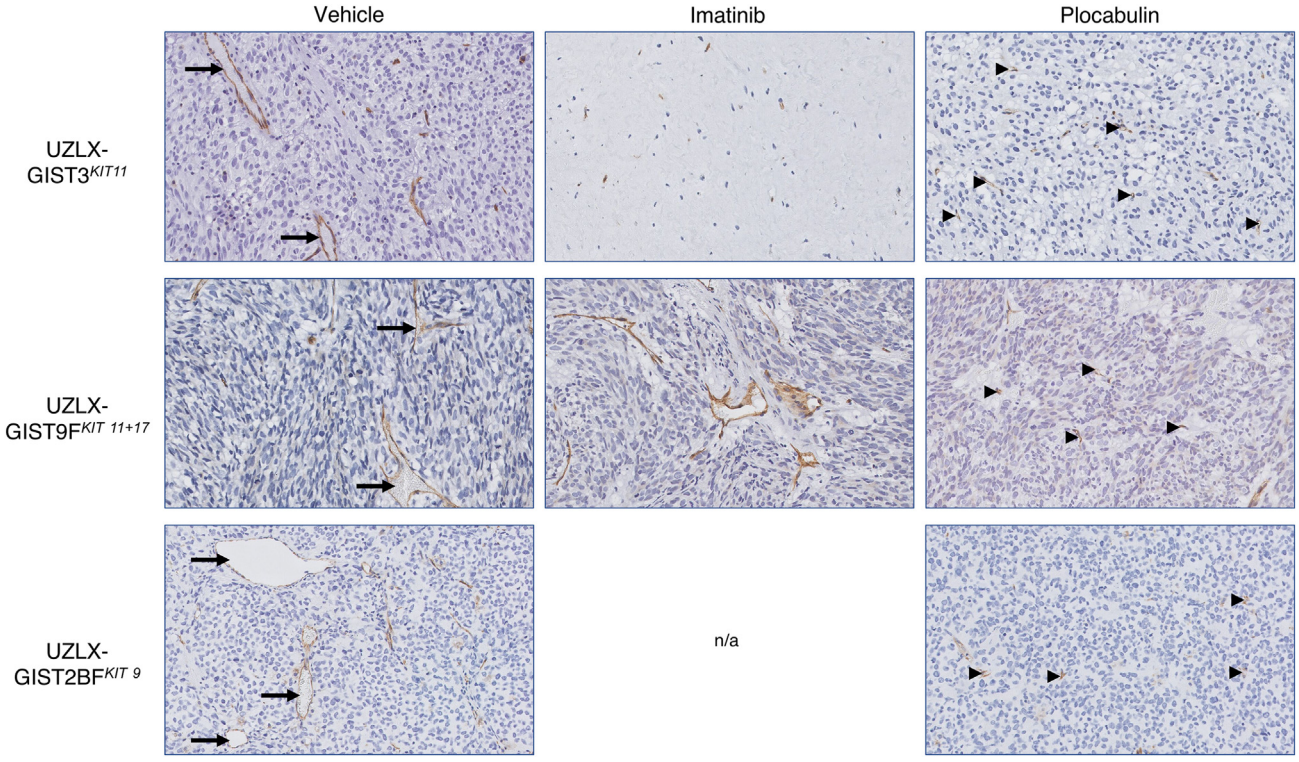

Fig. 5. Placobulin showed vascular-disruptive effects. Placobulin-treated tumors contained small, collapsed microvessels with barely discernable lumina (arrowheads) while vehicle-treated tumors contained large and dilated blood vessels, often filled with erythrocytes (arrows). Representative CD31-stains captured at 200× magnification. n/a: not available.

was able to disrupt the microtubule network of endothelial cells *in vitro*. This interference resulted in an altered morphology of those cells, a diminished ability of invasion and a disruption of any formed capillary-like network. Additionally, these vasodisruptive phenomena were also observed in xenograft models *in vivo*, where placobulin lead to a significant reduction in vascular volume and extensive necrosis. Interestingly, the vasodisruptive capacity of placobulin was concentration-dependent and occurred at concentrations lower than those affecting cell survival [29]. This may explain why in the current study we observed an antiangiogenic effect without a decisive effect on proliferation or apoptosis.

One limitation of the current study is the collection of tumor samples only at the very end of the experiment. Samples collected at this time point only allow histologic assessment of what remains after treatment. If the treatment proves to be effective, then tumors showing high levels of histologic response will be unsuited for the analysis of certain parameters, such as proliferation and apoptosis, as a result of the regressive changes. Collection of tissue during treatment, for example by biopsies, will enable the assessment of these tumors. Multiple collections of tissue during such an experiment will also lend to the assessment of the temporal effect of the drug, *i.e.*, how do the effects of the drug on different histological parameters evolve over the course of the treatment.

Another limitation of this study is whether our findings in PDX models can be translated to GIST in patients *in situ*. Human stromal cells, including endothelial cells and supplying microvessels, are rapidly replaced by murine ones after 3–5 passages [47]. Moreover, the microvessels that were assessed in this study were detected by a CD31 antibody that was specifically raised against the murine epitope, with no cross-reactivity to human CD31. Thus, the studied microvessels were of murine nature. Bearing in mind the vasodisruptive effects of placobulin, murine models may not be the best research platform to investigate its effects on tumor vasculature. It could be argued that microvessels of murine origin might be more sensitive to its vasodisruptive effects than human microvessels. However, the disruptive effects on endothelial cells *in vitro* reported previously were observed in endothelial cells of human origin [29]. Additionally, when taking into account the extent of necrosis that was observed in the current study, it seems that placobulin efficiently affects tumor vasculature of both human and murine origin.

We would like to point out that placobulin was tested at 16 mg/kg in the present study, as previous *in vivo* work demonstrated a good antitumor effect at this dose [28,29]. However, this corresponds to a human equivalent dose of 1.3 mg/kg or 48 mg/m^2 [47], well above 9.3 mg/m^2 that is being evaluated in the current clinical trials [30,31]. Thus, it remains unclear whether the dose tested in the current study can be achieved in human without severe toxicity. Additionally, the recent phase I study demonstrated the maximum tolerated dose of placobulin to be 14.5 mg/m^2 and suggested that the recommended dose may be within the range of 9.3 mg/m^2 to 11.6 mg/m^2. The main dose limiting toxicity identified was peripheral sensory neuropathy, a side effect that is typically associated with tubulin-inhibiting agents. This side effect is often dose-dependent and not easily observed in rodent models. However, it remains unclear whether single agent doses of placobulin would actually be required for the clinical treatment of GIST. The vascular disruptive effects that we observed were so pronounced that it is likely that they would occur at even lower drug exposure. Additionally, a preserved vasculature is required for efficient drug delivery to tumors. Moreover, it may be that the tubulin inhibitor can be administered at a lower dose when considering a combination therapy with established TKI.

Due to their different and complementary mechanisms of action, placobulin could be combined with established TKI to enhance disease control in GIST, or to overcome resistance to kinase inhibitors. Mechanisms responsible for clinical progression in *KIT*-mutated GIST commonly involve the emergence of tumor cell subpopulations with heterogeneous, secondary mutations in *KIT*. These polyclonal populations ultimately expand and eventually result in clinically relevant disease progression. Taking into account this mechanism, adding placobulin to a treatment regimen with established TKI may enable to target these resistant clones, or to delay/prevent the occurrence of resistance. Conversely, adding TKI to a treatment regimen with placobulin may also enable to target the residual, albeit

small, viable tumor rim that remains after plocabulin treatment. Despite the extensive central tumor necrosis observed, this residual rim can act as a source of tumor regrowth or sanctuary site for the tumor cells, eventually also leading to disease progression [46]. This hypothesis of potential synergistic effects of combination therapy could be explored *in vivo* with an efficacy experiment, followed by a regrowth study after discontinuation of the experimental treatment. The efficacy experiment will allow for the evaluation of the combination therapy's efficacy and to find the optimal doses whereas the regrow experiment will allow for the assessment of any additional benefits to disease control in the longer term.

In conclusion, to our knowledge, this is the first study to evaluate the efficacy of a tubulin inhibitor in PDX models of GIST and the first *in vivo* study to assess the novel drug plocabulin in GIST. We demonstrated activity of the novel tubulin inhibitor in imatinib-sensitive and imatinib-resistant GIST, traditionally considered to be resistant to chemotherapy clinically. Our results challenge this established view that GIST are resistant to cytotoxic agents in general and to tubulin inhibitors in particular. We provide a convincing preclinical rationale for early clinical exploration of plocabulin in GIST, either as a single agent or in combination with established TKI.

Author contribution statement

Yannick Wang: Formal analysis, Investigation, Writing - Original Draft, Visualization, Validation; Agnieszka Wozniak: Conceptualization, Methodology, Investigation, Writing - Review & Editing, Supervision, Project administration, Funding acquisition; Jasmien Wellens: Investigation, Writing - Review & Editing; Yemarshet K. Gebreyohannes: Methodology; Maria Jose Guillén: Methodology; Pablo M. Avilés: Resources, Funding acquisition, Writing - Review & Editing, Methodology; Maria Debiec-Rychter: Methodology; Raf Sciot: Methodology, Supervision; Patrick Schöffski: Conceptualization, Supervision, Writing - Review & Editing, Funding acquisition.

Funding

This work was supported by PharmaMar S.A., Spain [R&D 2017/1052].

Prior presentation

A part of the results of this study has been presented as an abstract at the Connective Tissue Oncology Society Annual Meeting 2018 (November 14–17, 2018, Rome, Italy).

Declaration of competing interest

Yannick Wang received travel support from PharmaMar. Maria Jose Guillén and Pablo M. Avilés are employees of PharmaMar. Patrick Schöffski received institutional support from PharmaMar for research funding. Other authors declare no potential conflicts of interest.

Appendix A. Supplementary data

Supplementary data to this article can be found online at https://doi.org/10.1016/j.tranon.2020.100832.

References

[1] A. Rammohan, J. Sathyanesan, K. Rajendran, A. Pitchaimuthu, S.-K. Perumal, U. Nivasan, et al., A gist of gastrointestinal stromal tumors: a review, World J Gastrointest Oncol. 5 (2013) 102–112.
[2] N. Eng-Hen, R.E. Pollock, M.F. Munsel, E.N. Atkinson, M.M. Rodahl, Prognostic factors influencing survival in gastrointestinal leiomyosarcomas implications for surgical management and staging, Ann. Surg. 215 (1992) 68–77.
[3] R.P. DeMatteo, J.J. Lewis, D. Leung, S.S. Mudan, J.M. Woodruff, M.F. Brennan, Two hundred gastrointestinal stromal tumors, Ann. Surg. 231 (2000) 51–58.
[4] M. Sarlomo-Rikala, A. Kovatich, A. Barusevicius, M. Miettinen, CD117: a sensitive marker for gastrointestinal stromal tumors that is more specific than CD34, Mod. Pathol. 11 (1998) 728–734.
[5] S. Hirota, K. Isozaki, Y. Moriyama, K. Hashimoto, T. Nishida, S. Ishiguro, et al., Gain-of-function mutations of c-*kit* in human gastrointestinal stromal tumors, Science 279 (1998) 577–580.
[6] G.D. Demetri, M. von Mehren, C.D. Blanke, A.D. den Abbeele, B. Eisenberg, P.J. Roberts, et al., Efficacy and safety of imatinib mesylate in advanced gastrointestinal stromal tumors, N. Engl. J. Med. 347 (2002) 472–480.
[7] H. Joensuu, P.J. Roberts, M. Sarlomo-Rikala, L.C. Andersson, P. Tervahartiala, D. Tuveson, et al., Effect of the tyrosine kinase inhibitor STI571 in a patient with a metastatic gastrointestinal stromal tumor, N. Engl. J. Med. 344 (2001) 1052–1056.
[8] C.L. Corless, C.M. Barnett, M.C. Heinrich, Gastrointestinal stromal tumours: origin and molecular oncology, Nat. Rev. Cancer 11 (2011) 865–878.
[9] A. Wozniak, P. Rutkowski, P. Schöffski, I. Ray-Coquard, I. Hostein, H.-U. Schildhaus, et al., Tumor genotype is an independent prognostic factor in primary gastrointestinal stromal tumors of gastric origin: a European multicenter analysis based on ConticaGIST, Clin. Cancer Res. 20 (2014) 6105–6116.
[10] I. Hompland, Ø. Bruland, T. Hølmebakk, J. Poulsen, S. Stoldt, K. Hall, et al., Prediction of long-term survival in patients with metastatic gastrointestinal stromal tumor: analysis of a large, single-institution cohort, Acta Oncol. 56 (2017) 1–7.
[11] C. Serrano, A. Mariño-Enríquez, D.L. Tao, J. Ketzer, G. Eilers, M. Zhu, et al., Complementary activity of tyrosine kinase inhibitors against secondary kit mutations in imatinib-resistant gastrointestinal stromal tumours, Brit J Cancer. 120 (2019) 612–620.
[12] C.-M. Wang, K. Huang, Y. Zhou, C.-Y. Du, Y.-W. Ye, H. Fu, et al., Molecular mechanisms of secondary imatinib resistance in patients with gastrointestinal stromal tumors, J. Cancer Res. Clin. Oncol. 136 (2010) 1065–1071.
[13] H. Joensuu, P. Hohenberger, C.L. Corless, Gastrointestinal stromal tumour, Lancet 382 (2013) 973–983.
[14] G.D. Demetri, P. Reichardt, Y.-K. Kang, J.-Y. Blay, P. Rutkowski, H. Gelderblom, et al., Efficacy and safety of regorafenib for advanced gastrointestinal stromal tumours after failure of imatinib and sunitinib (GRID): an international, multicentre, randomised, placebo-controlled, phase 3 trial, Lancet 381 (2013) 295–302.
[15] G.D. Demetri, C.R. Garrett, P. Schöffski, M.H. Shah, J. Verweij, S. Leyvraz, et al., Complete longitudinal analyses of the randomized, placebo-controlled, phase III trial of sunitinib in patients with gastrointestinal stromal tumor following imatinib failure, Clin. Cancer Res. 18 (2012) 3170–3179.
[16] ClinicalTrials.gov [Internet]. Bethesda (MD): National Library of Medicine (US). 2000 -. Identifier NCT03465722. (VOYAGER) Study of Avapritinib vs Regorafenib in patients with locally advanced unresectable or metastatic GIST; 2019 [cited 2019 Oct 12]. Available from: https://clinicaltrials.gov/ct2/show/NCT03465722
[17] ClinicalTrials.gov [Internet]. Bethesda (MD): National Library of Medicine (US). 2000 -. Identifier NCT03673501. A study of DCC-2618 vs sunitinib in advanced GIST patients after treatment with imatinib (intrigue); 2019 [cited 2019 Oct 12]. Available from: https://clinicaltrials.gov/ct2/show/NCT03673501
[18] Y.-K. Kang, M.-H. Ryu, C. Yoo, B.-Y. Ryoo, H. Kim, J. Lee, et al., Resumption of imatinib to control metastatic or unresectable gastrointestinal stromal tumours after failure of imatinib and sunitinib (RIGHT): a randomised, placebo-controlled, phase 3 trial, Lancet Oncol. 14 (2013) 1175–1182.
[19] B. Vincenzi, M. Nannini, G. Badalamenti, G. Grignani, E. Fumagalli, S. Gasperoni, et al., Imatinib rechallenge in patients with advanced gastrointestinal stromal tumors following progression with imatinib, sunitinib and regorafenib, Ther Adv Med Oncol. 10 (2018) 1–8.
[20] J.H. Edmonson, R.S. Marks, J.C. Buckner, M.R. Mahoney, Contrast of response to dacarbazine, mitomycin, doxorubicin, and cisplatin (DMAP) plus GM-CSF between patients with advanced malignant gastrointestinal stromal tumors and patients with other advanced leiomyosarcomas, Cancer Investig. 20 (2002) 605–612.
[21] B.E. Plaat, H. Hollema, W.M. Molenaar, G.H. Broers, J. Pijpe, M.F. Mastik, et al., Soft tissue leiomyosarcomas and malignant gastrointestinal stromal tumors: differences in clinical outcome and expression of multidrug resistance proteins, J. Clin. Oncol. 18 (2000) 3211–3220.
[22] J. Verweij, P.G. Casali, J. Zalcberg, A. Lecesne, P. Reichardt, J.-Y. Blay, et al., Progression-free survival in gastrointestinal stromal tumours with high-dose imatinib: randomised trial, Lancet 364 (2004) 1127–1134.
[23] Casali P, Abecassis N, Bauer S, Biagini R, Bielack S, Bonvalot S, et al. Gastrointestinal stromal tumours: ESMO–EURACAN Clinical Practice Guidelines for diagnosis, treatment and follow-up. Ann Oncol. 2018; 29(Suppl 4):iv267.
[24] S. Boichuk, D.J. Lee, K.R. Mehalek, K.R. Makielski, A. Wozniak, D.S. Seneviratne, et al., Unbiased compound screening identifies unexpected drug sensitivities and novel treatment options for gastrointestinal stromal tumors, Cancer Res. 74 (2014) 1200–1213.
[25] M. Martín, L. Coello, R. Fernández, F. Reyes, A. Rodríguez, C. Murcia, et al., Isolation and first total synthesis of PM050489 and PM060184, two new marine anticancer compounds, J. Am. Chem. Soc. 135 (2013) 10164–10171.
[26] B. Pera, I. Barasoain, A. Pantazopoulou, A. Canales, R. Matesanz, J. Rodriguez-Salarichs, et al., New interfacial microtubule inhibitors of marine origin, PM050489/PM060184, with potent antitumor activity and a distinct mechanism, ACS Chem. Biol. 8 (2013) 2084–2094.
[27] A.E. Prota, K. Bargsten, F.J. Diaz, M. Marsh, C. Cuevas, M. Liniger, et al., A new tubulin-binding site and pharmacophore for microtubule-destabilizing anticancer drugs, Proc. Natl. Acad. Sci. U. S. A. 111 (2014) 13817–13821.
[28] M. Martínez-Díez, M. Guillén-Navarro, B. Pera, B. Bouchet, J. Martínez-Leal, I. Barasoain, et al., PM060184, a new tubulin binding agent with potent antitumor activity including P-glycoprotein over-expressing tumors, Biochem. Pharmacol. 88 (2014) 291–302.
[29] C.M. Galmarini, M. Martin, B. Bouchet, M. Guillen-Navarro, M. Martínez-Diez, J. Martinez-Leal, et al., Plocabulin, a novel tubulin-binding agent, inhibits angiogenesis by modulation of microtubule dynamics in endothelial cells, BMC Cancer 18 (2018) 164.
[30] ClinicalTrials.gov [Internet]. Bethesda (MD): National Library of Medicine (US). 2000 -. Identifier NCT03427268. Clinical trial of PM60184 in advanced colorectal cancer after

standard treatment; 2018 [cited 2019 Oct 12]. Available from: https://clinicaltrials.gov/ct2/show/NCT03427268
[31] EudraCT [Internet]. Amsterdam: European Medicines Agency (NL). 2004 -. Identifier 2015-002395-24. Phase II, open-label, randomized, controlled study of PM060184 in advanced, hormone receptor positive, HER2 negative breast cancer patients in third or fourth line setting; 2018 [cited 2019 Oct 12]. Available from: https://www.clinicaltrialsregister.eu/ctr-search/search?query=2015-002395-24
[32] ClinicalTrials.gov [Internet]. Bethesda (MD): National Library of Medicine (US). 2000 -. Identifier NCT01299636. Study of PM060184 in patients with advanced solid tumors; 2015 [cited 2019 Oct 12]. Available from: https://clinicaltrials.gov/ct2/show/NCT01299636
[33] ClinicalTrials.gov [Internet]. Bethesda (MD): National Library of Medicine (US). 2000 -. Identifier NCT02533674. Multicenter, open-label, clinical and pharmacokinetic study of PM060184 in combination with gemcitabine in selected patients with advanced solid tumors; 2017 [cited 2019 Oct 12]. Available from: https://clinicaltrials.gov/ct2/show/NCT02533674
[34] G. Floris, M. Debiec-Rychter, R. Sciot, C. Stefan, S. Fieuws, K. Machiels, et al., High efficacy of panobinostat towards human gastrointestinal stromal tumors in a xenograft mouse model, Clin. Cancer Res. 15 (2009) 4066–4076.
[35] C.R. Antonescu, P. Besmer, T. Guo, K. Arkun, G. Hom, B. Koryotowski, et al., Acquired resistance to imatinib in gastrointestinal stromal tumor occurs through secondary gene mutation, Clin. Cancer Res. 11 (2005) 4182–4190.
[36] J. Going, Counting cells made easier, Histopathology 49 (2006) 309–311.
[37] N. Weidner, J.P. Semple, W.R. Welch, J. Folkman, Tumor angiogenesis and metastasis — correlation in invasive breast carcinoma, N. Engl. J. Med. 324 (1991) 1–8.
[38] G. Floris, A. Wozniak, R. Sciot, H. Li, L. Friedman, T. Looy, et al., A potent combination of the novel PI3k inhibitor, GDC-0941, with imatinib in gastrointestinal stromal tumor xenografts: long-lasting responses after treatment withdrawal, Clin. Cancer Res. 19 (2013) 620–630.
[39] J. Cornillie, A. Wozniak, H. Li, Y. Wang, B. Boeckx, Y.K. Gebreyohannes, et al., Establishment and characterization of histologically and molecularly stable soft-tissue sarcoma xenograft models for biological studies and preclinical drug testing, Mol. Cancer Ther. 18 (2019) 1168–1178.
[40] T. Looy, Y. Gebreyohannes, A. Wozniak, J. Cornillie, J. Wellens, H. Li, et al., Characterization and assessment of the sensitivity and resistance of a newly established human gastrointestinal stromal tumour xenograft model to treatment with tyrosine kinase inhibitors, Clin Sarcoma Res. 4 (2014) 10.
[41] Y.K. Gebreyohannes, A. Wozniak, M.-E. Zhai, J. Wellens, J. Cornillie, U. Vanleeuw, et al., Robust activity of avapritinib, potent and highly selective inhibitor of mutated kit, in patient-derived xenograft models of gastrointestinal stromal tumors, Clin Cancer Res. 25 (2019) 609–618.
[42] Y.K. Gebreyohannes, P. Schöffski, T. Looy, J. Wellens, L. Vreys, J. Cornillie, et al., Cabozantinib is active against human gastrointestinal stromal tumor xenografts carrying different KIT mutations, Mol Cancer Ther. 15 (2016) 2845–2852.
[43] T. Looy, A. Wozniak, G. Floris, H. Li, J. Wellens, U. Vanleeuw, et al., Therapeutic efficacy assessment of CK6, a monoclonal kit antibody, in a panel of gastrointestinal stromal tumor xenograft models, Transl Oncol. 8 (2015) 112–118.
[44] D. Mili, K. Abid, I. Rjiba, A. Kenani, Effect of SP600125 on the mitotic spindle in HeLa cells, leading to mitotic arrest, endoreduplication and apoptosis, Mol. Cytogenet. 9 (2016) 86.
[45] C. Prigent, S. Dimitrov, Phosphorylation of serine 10 in histone H3, what for? J. Cell Sci. 116 (2003) 3677–3685.
[46] J.H. Gill, K.L. Rockley, C. Santis, A.K. Mohamed, Vascular disrupting agents in cancer treatment: cardiovascular toxicity and implications for co-administration with other cancer chemotherapeutics, Pharmacol. Ther. 202 (2019) 18–31.
[47] M. Hidalgo, F. Amant, A.V. Biankin, E. Budinská, A.T. Byrne, C. Caldas, et al., Patient-derived xenograft models: an emerging platform for translational cancer research, Cancer Discov. 4 (2014) 998–1013.